ChemElectroChem

Research Article
doi.org/10.1002/celc.202300485

Chemistry Europe
European Chemical Societies Publishing

www.chemelectrochem.org

Enhancing the Oxygen Evolution Reaction Activity of Sputtered Ni, NiO, and NiNiO Thin Films by Incorporating Fe

Megan Muriel Heath,[a] Marcelle Potgieter,[a] Frode Seland,[b] Svein Sunde,*[b] and Roelof Jacobus Kriek*[a]

The effect of Fe-containing alkaline electrolyte, on the oxygen evolution reaction (OER) activity of Ni electrocatalysts, has long been of interest as Fe increases the OER activity of Ni electrocatalysts. However, controversy exists as to whether it is surface or bulk Fe that is responsible for the increased activity. In this study, magnetron sputtering was employed to sputter Ni, NiO and NiNiO thin film electrocatalysts to study the effect that different concentrations of Fe in the electrolyte have on their OER activities. It was found that increasing concentrations of Fe increasingly enhanced the OER activity of these thin film electrocatalysts until the electrolyte was saturated with Fe. The lowest overpotential achieved is 279 mV (at 10 mA cm^{-2}) for NiNiO cycled in KOH containing 1 mM Fe, with all three thin film electrocatalysts exhibiting overpotentials within the same range after 30 voltammetry cycles in 0.9 ppm Fe and 1 mM Fe. All Tafel slopes are between 36 and 45 mV dec^{-1} indicating similar kinetics for the samples cycled in different Fe concentrations. Energy-dispersive X-ray spectroscopy and X-ray photoelectron spectroscopy results show that Fe is found in the top layers of the electrocatalysts after cycling.

Introduction

Alkaline water electrolysis is a well-established method for converting and storing energy in the form of hydrogen, which involves two half-cell reactions, the hydrogen evolution reaction (HER) and the oxygen evolution reaction (OER). One of the main challenges of this process is the high overpotential required for the OER, which limits the overall efficiency and cost-effectiveness of the technology. To address this issue, transition metal electrocatalysts, such as Ni, have been extensively studied to reduce the OER overpotential. In particular, the addition of Fe has been found to significantly enhance the OER activity of Ni electrocatalysts, a phenomenon described as the "Fe-effect" in a recent review.[1]

Despite Fe's slow OER kinetics and poor conductivity,[2] its positive effect on the OER activity of Ni has long been known and recent studies have demonstrated its potential to improve the performance of Ni electrocatalysts in a controlled way.[3–5] In the classical work by Corrigan, it was revealed that trace amounts of Fe in the electrolyte dramatically impact the OER activity of Ni electrodes.[6] Fe unintentionally incorporates into the Ni film from impurities in the electrolyte during potential cycling, resulting in increased OER activity.[6] Yeo and Bell studied $\alpha - Ni(OH)_2$ aged in concentrated reagent grade KOH to obtain $\beta - Ni(OH)_2$.[7] The increased OER activity and changes in Raman features ascribed to $\beta - Ni(OH)_2$/ β-NiOOH in their study could be due to unintentional Fe incorporation from the reagent grade KOH electrolyte. There are many more examples of studies that report excellent activity for Ni electrodes when unpurified KOH was used, with the high activity resulting from unintentional Fe incorporation. One example is by Stern and Hu who found that $Ni(OH)_2$ nanoparticles exhibited excellent OER activity with an overpotential at 10 mA cm^{-1} of only 299 mV.[8] They repeated the experiment for the $Ni(OH)_2$ nanoparticles in purified KOH and found a drastic decline in OER activity. They therefore concluded that Fe impurities that incorporate into NiOOH to form $Ni_xFe_{1-x}OOH$ as active phase is critical for achieving excellent OER activities.[8] Furthermore, Klaus *et al.* conducted a study of Ni in both purified and reagent grade KOH to evaluate this effect of unintentional Fe incorporation on the associated structure (in-situ Raman spectroscopy) and OER activity (cyclic voltammetry).[4] This study reported a dramatic decrease in Tafel slope as well as overpotential when the Ni electrodes were aged in non-purified reagent grade KOH for 6 days, which was comparable to values of Ni–Fe catalysts.

Aside from incidental incorporation of Fe from unpurified KOH, some studies spike the electrolyte with known concentrations of Fe to observe the effect thereof on OER activity of Ni. In their work using reagent grade KOH and KOH saturated with Fe(~0.7 mM Fe), Nardi *et al.* observed changes in the OER activity after potential cycling and related it to the structure of NiO_x films after cycling.[9] They observed overpotentials of

[a] M. M. Heath, M. Potgieter, Prof. R. J. Kriek
Electrochemistry for Energy & Environment Group, Research Focus Area: Chemical Resource Beneficiation (CRB), North-West University, Private Bag X6001, Potchefstroom 2520, South Africa
E-mail: cobus.kriek@nwu.ac.za

[b] Prof. F. Seland, Prof. S. Sunde
Department of Materials Science and Engineering, Norwegian University of Science and Technology (NTNU), Trondheim NO-7491, Norway
E-mail: svein.sunde@ntnu.no

Supporting information for this article is available on the WWW under https://doi.org/10.1002/celc.202300485

0.54 V and 0.48 V at 10 mA cm^{-2} for the NiO_x films cycled at 20 mV s^{-1} in reagent grade and Fe saturated 0.1 M KOH, respectively.[9] Interestingly, while the OER activity of the film cycled in saturated KOH was higher, this film had a smaller electrochemically active surface area (ECSA).[9] Furthermore, both cyclic voltammetry (CV) and X-ray photoelectron spectroscopy (XPS) results in their study indicate that a high Fe concentration limits the amount of oxidation occurring at the NiO_x surface during electrochemical potential cycling.[9] They also found that Fe incorporation is not dependent on applied potential but is rather a diffusion-limited process.[9] These effects of Fe incorporation are interesting and important towards OER electrocatalyst development, and similar studies were subsequently conducted by several groups. Burke Stevens *et al.* spiked a pure KOH solution with 1 mM $Fe(NO_3)_3$ and found an immediate increase in OER activity for a $Ni(OH)_2$ catalyst cycled in the solution.[5] The overpotential showed a 130–150 mV decrease along with an anodic shift of the oxidation peak (E_{pa}) and a decreased integrated area of this peak.[5] After 100 cycles, they performed inductively coupled plasma optical emission spectroscopy (ICP-OES) analysis and found that the film contained 23–25% Fe.[5] This is slightly higher than the 10–15% Fe that the NiO_x film in the study by Nardi *et al.* contained after cycling in a similar amount of Fe.[9] However, less cycles were performed, consequently providing less time for Fe incorporation. Another study showed that the OER activity of co-electrodeposited NiFe electrocatalysts is enhanced with increasing Fe concentration, up to 10% Fe, and that the overpotential does not vary much between 15% and 50% Fe.[10] This also agrees with the study performed by Landon *et al.* where it was observed that 10 mol% Fe yielded optimum OER activities for mixed NiFe.[11] Therefore, there plausibly exists a saturation point where the activity of Ni electrocatalysts cannot be enhanced further with increasing Fe concentrations.

The exact mechanism behind this effect is not yet fully understood, and there is ongoing debate about whether bulk Fe or surface Fe is responsible for the increased activity. There are two main ways in which Fe can be incorporated into Ni electrocatalysts: in the surface or in the bulk. Bulk Fe replaces some of the Ni in the $Ni(OH)_2$ structure, resulting in a structure known as NiFe layered double hydroxide (NiFe LDH).[12] Surface Fe, on the other hand, is initially adsorbed on the electrocatalyst surface at various sites.[12] Recent studies have suggested that surface Fe is the more active species in Ni electrocatalysts and that the OER takes place exclusively at the near-surface region of the electrocatalysts.[9,12–14]

Ni electrocatalysts have been synthesized and studied in various forms and phases, including metallic/polycrystalline polished Ni,[15–18] sputtered Ni,[19,20] electrodeposited variants,[4,3,21] and various morphologies of Ni nanoparticles.[22–29] These electrocatalysts often include various phases of Ni, such as oxides and hydroxides, which can impact their OER performance. The higher oxidation states of Ni, such as Ni^{2+} or Ni^{3+}, are generally considered to be more active for OER,[30–32] and therefore, materials such as NiO and $Ni(OH)_2$ are commonly used.[7,30,33–35]

In studying the effect of Fe on Ni electrocatalysts, reproducibility and sample preparation time are two potential challenges. Physical vapor deposition (PVD), specifically magnetron sputtering, has been widely used to produce thin film electrocatalysts with tailored compositions.[19,36–38] By using PVD one has the possibility to obtain very thin films that closely resembles bulk properties. This method can improve the reproducibility of samples and produce materials that more closely resemble bulk materials than nanoparticles.

This study explored the use of sputtered Ni, NiO, and NiNiO thin films as electrocatalysts for the oxygen evolution reaction (OER) in Fe-doped alkaline electrolyte. The different Ni oxidation states were used to evaluate if the oxidation state affects Fe incorporation. NiNiO is chosen as a mixed oxidation state. The electrocatalysts were directly sputtered onto polished glassy carbon (GC) electrodes and were characterized using electrochemical and physical characterization techniques, such as energy-dispersive X-ray spectroscopy (EDX) and X-ray photoelectron spectroscopy (XPS). It was found that increasing Fe content in the electrolyte enhances the OER activity, reaching a limit when the electrolyte is supersaturated with Fe. It also gives an indication that surface Fe, rather than Fe incorporated within the bulk structure, was responsible for the enhanced OER activity.

Methods

Sputtering Ni, NiO and NiNiO thin films

Before sputtering the thin films, GC disks (Sigradur G, HTW Germany) were prepared as substrates. After rough polishing on carbon pads, the GC disks were polished on microfiber polishing pads with 0.3 μm and 0.05 μm alumina suspensions (Allied High-Tech Products, Inc.). In between polishing, with the two different particle sizes, the disks were rinsed with water (18.2 MΩ.cm, Milli-Q water). Lastly, the disks were consecutively sonicated in water, 1 M pure KOH and isopropyl alcohol (IPA) (technical, VWR) for 10 minutes in each solvent.

Pure Ni, NiO and NiNiO films were magnetron sputtered onto polished GC substrates using a custom-made PVD system (PVD products, USA). A pure Ni target (99.99% from ACI Alloys, Inc.) as well as a NiO target (99.99% from ACI Alloys, Inc.), was used to deposit these thin films under ultra-high vacuum (UHV) conditions. The thin films containing Ni were sputtered employing Direct Current magnetron sputtering. The NiO target used to sputter NiNiO samples is sputtered employing radiofrequency (RF) power. Argon was used as the sputtering gas at an Ar flow rate of 0.025 L min^{-1} and a chamber pressure of 10 mTorr, the flow rate was calibrated. Accordingly, the calibration equation $y = 0.1171x - 0.3756$ was attained, where y represents the sputtering rate (nm/min), and x denotes the power (W). This equation was employed to determine the amount of time needed to sputter a 50 nm film. At 90 W power, a base pressure of 10 mTorr and an Ar flow rate of 0.025 L/min, 5 min and 56 s of sputtering yielded uniform Ni films of 50 nm. NiO films were prepared by reactive sputtering with oxygen. The same conditions were used as described for the Ni films, with the only change being that oxygen was bled into the sputtering chamber at a flow rate of 0.005 L/min. It was subsequently found that reactively sputtered NiO resulted in severe delamination in KOH electrolyte when sputtered directly onto a polished GC electrode surface. To

solve this problem, a thin layer (10 nm) of Ni was sputtered onto the GC surface, followed by a 40 nm layer of reactively sputtered NiO. NiNiO was prepared by simultaneously using the Ni and NiO targets. Ni was sputtered at 90 W while NiO was simultaneously sputtered at 50 W, for 5 min and 56 s. Sputtered Ni and NiNiO films had a polished silver appearance whereas the sputtered NiO films had a glossy black colour with a blueish hue.

SEM and EDX

Scanning electron microscopy (SEM) (FEI Quanta FEG 250) with an integrated XMax 20 energy dispersive x-ray (EDX) system (Oxford instruments) was used to determine the compositions of the sputtered thin films semi-quantitatively. Since the sputtered thin films are amorphous and extremely thin, x-ray diffraction (XRD) could not be used as a physical characterization technique to analyze the compositions of these samples. Therefore, EDX is a feasible alternative to evaluate if the desired compositions have been sputtered. Furthermore, the samples were also subjected to EDX after cycling in electrolytes that contain different amounts of Fe. For this, three to five different spots on the electrode surfaces were analyzed to obtain an average Fe concentration. EDX mapping was also conducted on the entire electrode surface to visualize the distribution of Ni and O, as well as Fe, after cycling.

XPS

X-ray photoelectron spectroscopy (XPS) was conducted by employing an Axis Ultra DLD instrument (Kratos Analytical). A monochromatic Al Kα-source was employed for the XPS analysis of the sputtered thin films. CasaXPS (Casa Software, Ltd.) was employed to analyze the raw XPS data. The spectra were calibrated according to the C 1s peak at 284.8 eV for adventitious carbon.

Electrochemical characterization

A three-electrode electrochemical cell was used for all electrochemical analyses. The experiments were conducted in a water-jacketed Teflon-lined cell at 25 °C, employing a Julabo F25 water bath for the jacketed Teflon cell. The electrodes were connected to a BioLogic (VMP3) potentiostat controlled by EC-Lab software. GC disks with sputtered Ni, NiO, or NiNiO thin films on their surface, were inserted into an interchangeable rotating disk electrode (RDE), which served as the working electrode (WE) for electrochemical analysis. The GC WE was used as part of an RDE setup (Pine Research). A Pt counter electrode (CE) (periodically cleaned by submerging in aqua regia for 1 minute) and a Hg/HgO reference electrode (RE) (Pine Research) was used. Calibration of the RE was performed by using a CV scan (10 $mV\,s^{-1}$ between −1.0 V and 0.9 V) in hydrogen saturated 0.1 M KOH with Pt serving as the WE and CE.[39] The voltage intercept of the forward and backward scans was averaged, and 0.87 V was obtained as the offset potential that was used to convert all measured potentials to the RHE scale according to $E_{RHE} = E_{measured} - E_{offset}$.

0.1 M KOH was used as electrolyte. KOH (semiconductor grade KOH pellets, 99.99%, Sigma Aldrich) was dissolved in deionized (DI) water (18.2 $M\Omega\,cm^{-1}$, 3 ppb TOC, Milli-Q water). This KOH could have required even further purification to be completely free of Fe, but is considered adequate for this study. This KOH, to which no additional iron was added, will henceforth be referred to as undoped KOH. To avoid Fe contamination for the Fe-free experiments, no glass equipment was used, and all the equipment was periodically cleaned with 1 M H_2SO_4 (95–97%, VWR). Iron(III) nitrate nonahydrate ($Fe(NO_3)_3 \cdot 9H_2O$, 99.9999% trace metals basis, Sigma Aldrich) was used to dope the electrolyte with different concentrations of Fe. The electrolyte was saturated with Ar to avoid any impact of oxygen on the redox features.

The ZIR function of EC-Lab software was used to correct for the ohmic (IR) drop in-situ by using 85% of the ohmic resistance measured before an experiment. To measure the ohmic resistance, the software performs an EIS experiment at high frequencies (0.1–10^5 Hz) and an alternating current (AC) perturbation amplitude of 10 mV.

For the OER the Gibbs energy change at 25 °C is 237.24 $kJ\,mol^{-1}$, and can be used to calculate the standard potential of the reaction as 1.23 V.[40] This value was subtracted from the measured IR-corrected potential to obtain the overpotential.

The current density is normalized with respect to the geometric surface area of the WE. The electrochemically active surface area (ECSA) will be influenced by Fe that is incorporated into the electrocatalyst, which will subsequently affect the reported current density. In addition, Fe is constantly being incorporated onto/into the electrocatalyst as different concentrations of Fe were added to the electrolyte. Therefore, the ECSA could be dynamically changing with each experiment as more Fe is incorporated. For this reason, to ensure consistency, the geometric surface area is used in this work. Measurements of the electrochemical double layer (EDL) capacitance were performed and can be found in the supporting information, along with experimental details on the technique.

Cyclic voltammetry (CV) was performed between 1 and 1.67 V vs RHE, at a scan rate of 20 $mV\,s^{-1}$, while the WE was rotated at 1600 rpm (revolutions per minute). This potential range was chosen as it allows for preconditioning, but at the same time shows the OER activity of the electrocatalysts. A scan rate of 20 $mV\,s^{-1}$ was chosen as it results in the production of stable CVs and as it takes a reasonable time to complete. Thirty CVs were performed between 1 and 1.67 V vs RHE, after which a linear sweep voltammogram (LSV) was recorded at 1 $mV\,s^{-1}$ within the same potential range. Lastly, EIS measurements to investigate the electrochemical behavior of the sputtered electrocatalysts were also conducted. The measurements were carried out at 1.485 V, 1.49 V, 1.495 V and 1.5 V vs RHE. The AC perturbation potential amplitude used was 10 mV, and the frequency range was 30 kHz to 0.1 Hz.

Tafel slopes were determined by employing chronoamperometry (CA) measurements at a rotation rate of 1600 rpm. In a CA experiment, potential steps are applied to the WE. The potential steps used were: 1.37, 1.42, 1.44, 1.47, 1.49, 1.51, 1.53, 1.55, 1.57, 1.59, 1.61, 1.63, 1.65 and 1.67 V. Each step was held for 30 seconds while the current response was recorded. In order to obtain current versus potential curves for Tafel analysis, the current response was plotted against each potential value. The overpotential was corrected for IR-drop before plotting it against the current density.

Results and discussion

SEM-EDX

From the SEM images (Figure S1) it is clear that sputtered thin films of Ni are uniform flat surfaces. NiO contains the highest percentage of oxygen (33.07%), and Ni the lowest percentage (7.58%). Oxygen will be present for pure Ni samples as it is well-known that a thin layer of NiO forms on the surface of a Ni electrode upon exposure to air.[15] The percentage of oxygen present for the as-prepared NiNiO (20.70%) falls between that

of Ni and NiO, showing that the intended mixture of Ni and NiO, to form NiNiO, is plausible. Secondly, the Fe concentrations of the sputtered thin films were analysed before and after cycling in electrolytes that contained different concentrations of Fe (Table S1). It is clear from the EDX results, for samples cycled in undoped KOH and 0.007 ppm Fe, that should Fe be present it is well below the detection limit. It is important to note that, in general, Fe concentrations vary greatly at different points of the same thin film. This shows that, during electrochemical cycling in Fe-containing electrolytes, Fe does not incorporate into the films homogeneously. EDX mapping (Figure S2) of Ni, NiO, and NiNiO surfaces, after cycling in 0.9 ppm Fe electrolyte, clearly shows the distribution of Fe across the electrode surface (in line with Table S1).

XPS

Initially, an XPS survey spectrum was acquired to identify the elements and impurities present in the sample (Figure S3). After the survey spectra have been collected, high resolution regional scans were performed of the Ni 2p, O 1s, Ni 3p and Fe 3p peaks. Figure 1 displays the Ni 2p XPS spectra of the as-prepared sputtered electrocatalyst along with the spectra of these electrocatalysts after cycling in undoped KOH, and KOH containing 0.007 ppm, 0.3 ppm, and 1 mM Fe. The Ni 2p XPS spectrum comprises Ni $2p_{3/2}$ (~850 to 860 eV) and Ni $2p_{1/2}$ (~870 to 875 eV) peaks due to multiplet splitting, as well as satellite peaks (~860 and 880 eV). These peaks show the oxidation states of the Ni samples, with Ni $2p_{3/2}$ being the most effective in indicating the oxidation states. The component peak at 855.5 eV corresponds to $Ni(OH)_2$,[9,41] the peak at 853.8 eV corresponds to NiO[41,42] and that at 852.48 eV, to Ni.[41,43,44] $Ni(OH)_2$ and NiO are present on the surface of sputtered Ni due to spontaneous reaction with oxygen in the atmosphere. For the sputtered NiO sample, the Ni^{2+} oxidation state (Ni $2p_{3/2}$) presents itself in two forms/peaks, i.e., a component peak at 855.4 eV, due to the presence of $Ni(OH)_2$, and the peak at 853.6 eV that is due to the presence of NiO. The fact that no metallic Ni is present indicates that NiO has been successfully prepared. The NiNiO sample contains metallic Ni (Ni^0 component peak at 852.1 eV) and Ni in the +2 oxidation state as NiO (853.6 eV) and $Ni(OH)_2$ (855.5 eV).

After cycling Ni in undoped KOH and 0.007 ppm Fe, only $Ni(OH)_2$ was present, whereas Ni samples cycled in 0.3 ppm Fe and 1 mM Fe exhibited not only $Ni(OH)_2$ peaks, but also small peaks corresponding to metallic Ni (~852 eV),[44,41,43] indicating less oxidation after cycling in higher Fe concentrations. This corresponds well with previous findings in literature.[9] The same observations can be made for NiO. The spectra shows that NiO contained more NiO with respect to $Ni(OH)_2$ as the Fe concentration increased. The NiO peak for the sample cycled in 0.007 ppm Fe is more or less the same size than that of the sample cycled in undoped KOH. However, for the sample cycled in 0.3 ppm Fe the peak at ~853 eV is larger, and the largest for the sample cycled in 1 mM Fe.

NiNiO samples cycled in KOH containing 0.007 ppm Fe and 1 mM Fe both contained small amounts of metallic Ni, evidenced by the small peak present at 852 eV in both of these spectra. NiNiO samples cycled in undoped KOH and KOH containing 0.3 ppm Fe only contained $Ni(OH)_2$ evidenced by a single Ni $2p_{3/2}$ component peak at 855.4 eV. This means that these samples are more oxidized than the samples cycled in 0.007 ppm and 1 mM Fe.

To gain a more accurate perspective of the oxidation states of the samples before and after cycling, high resolution scans of the O 1s peak was also obtained (Figure 2). Since no other oxygen containing components are present in these samples, the O 1s region would be a good reflection of the oxygen present on the surface of these samples. Three component peaks are seen for each of the sputtered samples. The peak at the highest binding energy (~532 eV) likely arises due to the presence of adsorbed water.[9] However, this peak has previously been ascribed to NiOOH.[45] It is difficult to exactly ascribe each peak to a specific bond, since Fe–O and Ni–O species also have very similar binding energies. However, previous studies of Ni electrocatalysts in Fe-containing electrolyte ascribed the peak at 531 eV to Ni–OH ($Ni(OH)_2$) and the peak at 529 eV to Ni–O (NiO).[9] Since it is also known that species occurring at higher binding energies are more oxidised, these spectra can show if the surfaces become more or less oxidised upon cycling in electrolytes containing different concentrations of Fe.

The O 1s XPS spectra for Ni show that the pristine sample and the sample cycled in 1 mM Fe have the highest concentrations of NiO, which is the least oxidized species. The concentrations of NiO in the samples cycled in undoped KOH and 0.007 ppm Fe are the same, and that of the sample cycled in 0.3 ppm Fe slightly higher. These results are in good agreement with the Ni 2p spectra in Figure 1 and the results of Nardi *et al.*, who found that Ni electrocatalysts that were exposed to potential cycling in an electrolyte containing concentrated amounts of Fe resulted in less oxidized surfaces, whereas cycling in lower Fe concentrations left the films more oxidized.[9] The same trend is observed for NiO, which is in line with the Ni 2p spectra that has been discussed earlier. The as-prepared sputtered NiO sample and the sample cycled in 1 mM Fe are the least oxidized. The sample cycled in 0.3 ppm Fe is slightly less oxidized compared to the samples cycled in undoped KOH and 0.007 ppm Fe, which are all more oxidized than the sample cycled in concentrated Fe. Lastly, the pristine NiNiO sample and the sample cycled in 1 mM Fe are the least oxidized, which again proves that cycling in concentrated Fe solutions causes the samples to be less oxidized. A possible explanation for this phenomenon is that the Fe on the surface is oxidized instead.

XPS was also used to quantify the amount of Fe present within the surface (approximately the top 5 nm) of the sputtered samples, before and after cycling. Ni Auger peaks rendered the Fe 2p peak impractical for quantification. Thus, high resolution scans of Ni 3p and Fe 3p peaks were used to quantify the XPS spectra of the sputtered Ni samples. As an example, Figure S4 shows the Ni 3p and Fe 3p peaks for the spot at the center of the surface of each sputtered Ni sample,

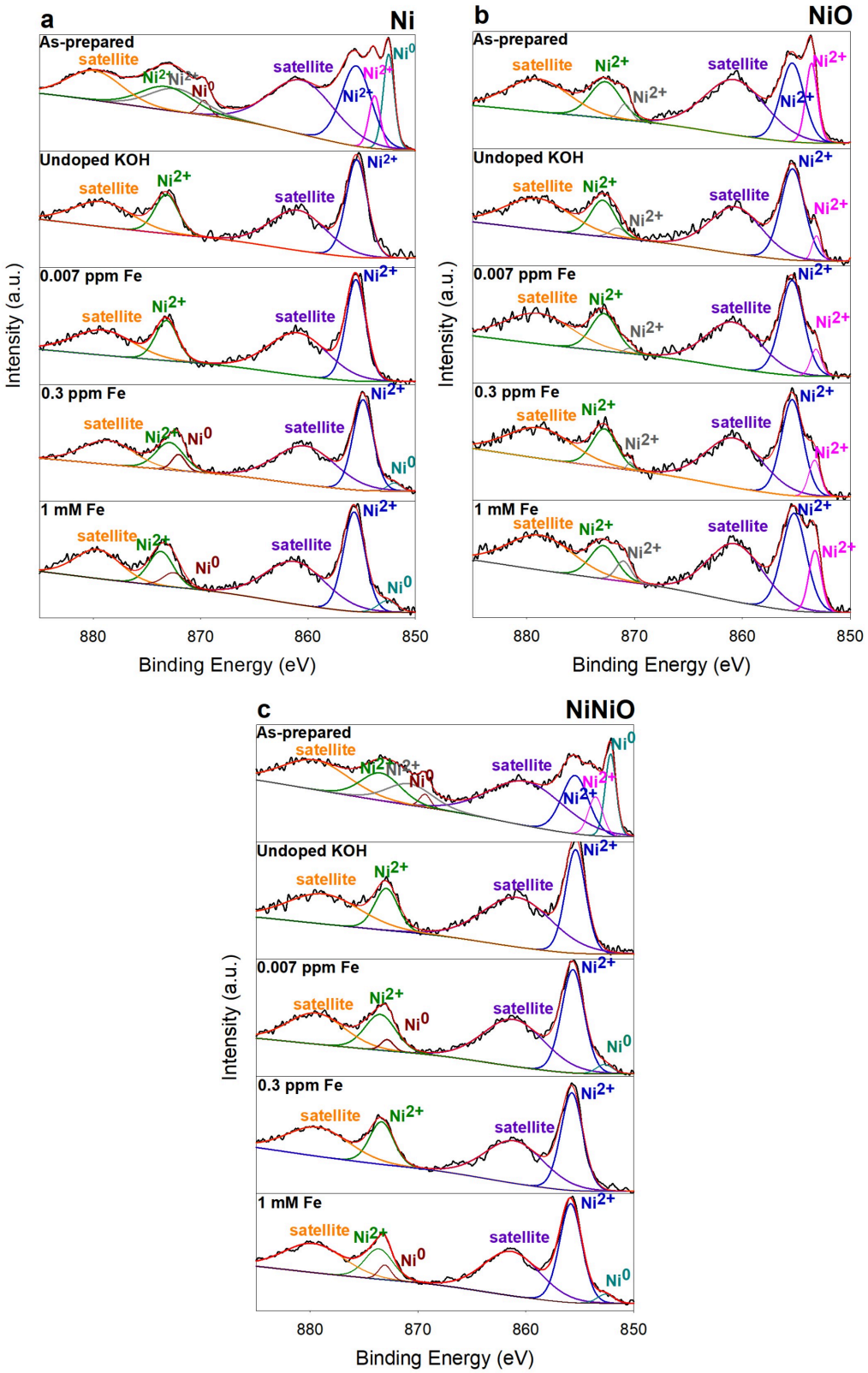

Figure 1. Ni 2p XPS spectra of sputtered (a) Ni, (b) NiO, and (c) NiNiO after 30 CV cycles in undoped KOH and KOH containing 0.007 ppm, 0.3 ppm and 1 mM Fe.

cycled in different concentrations of Fe as well as the pristine sample. Three spots on the surface of each sample were quantified to obtain an indication of the homogeneity of the Fe on the surface. The first spot is approximately at the center of

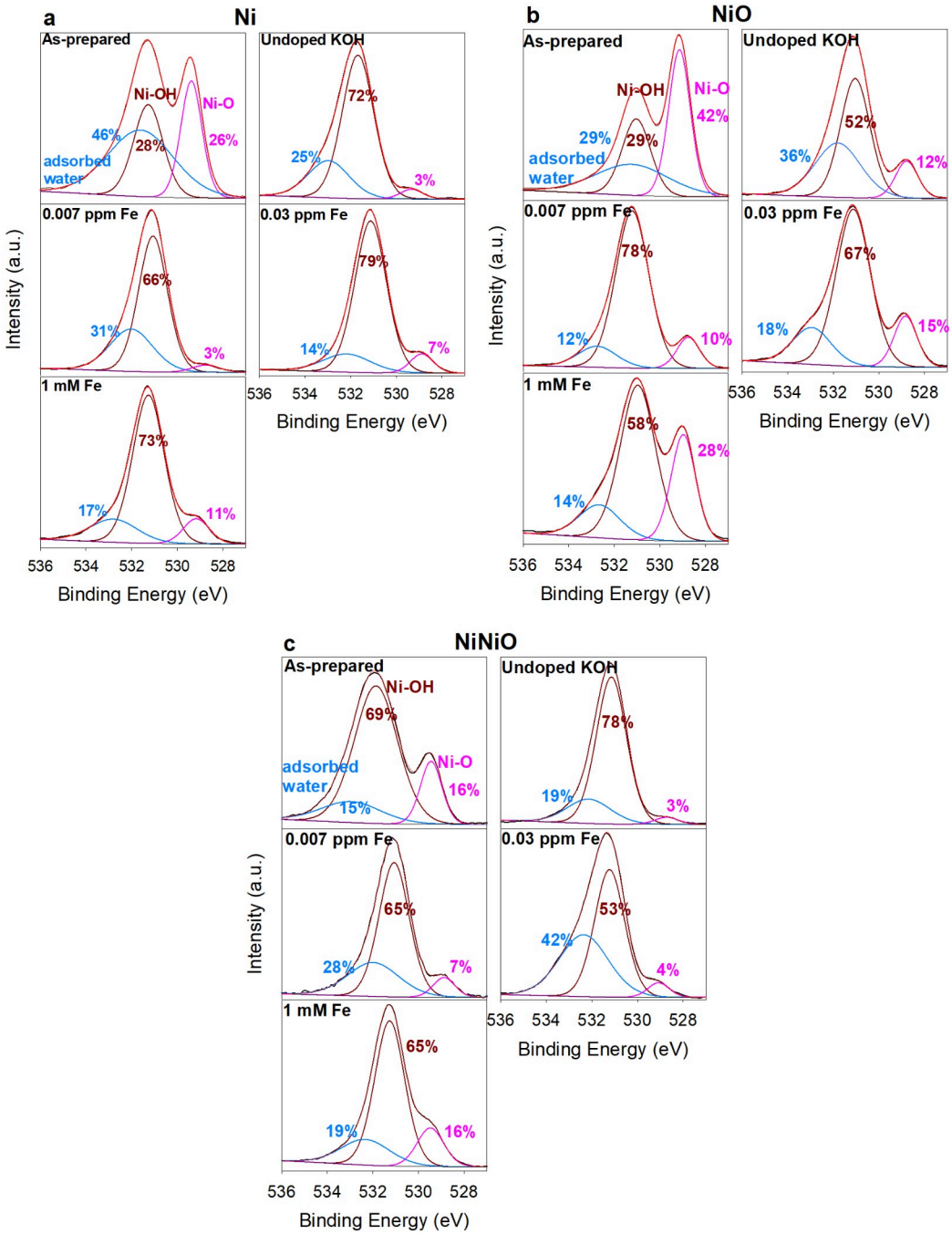

Figure 2. O 1 s XPS spectra of as-prepared sputtered (a) Ni, (b) NiO, and (c) NiNiO before and after 30 CV cycles in undoped KOH and KOH containing 0.007 ppm, 0.3 ppm and 1 mM Fe.

the sample, while the other two are each 1 mm away, so that the three points form a 90° angle. The bar charts representing these Fe concentrations on the surface of each sputtered sample can be seen in Figure S5.

The bar chart in Figure 3 indicates the average Fe concentrations in the top 5–10 nm of the film (or on the surface), as measured by XPS, versus average total concentrations (semi-quantitative) of Fe in the sample, as measured by EDX. The samples have been cycled in different Fe concentrations. The penetration depth of EDX (a few microns) is much deeper than that of XPS (roughly 5–10 nm). Therefore, EDX gives an indication of the total concentration of Fe within the sample (top layer and bulk), whereas XPS reflects only the top 5–10 nm. These EDX and XPS results show strong evidence that Fe is present mainly, or only, within the top 5–10 nm of the sputtered thin films, or on the surface. In our previous study we used in-situ Raman spectroscopy to show that Fe is present on the surface of nickel electrocatalyst samples as α-FeOOH.[46] The

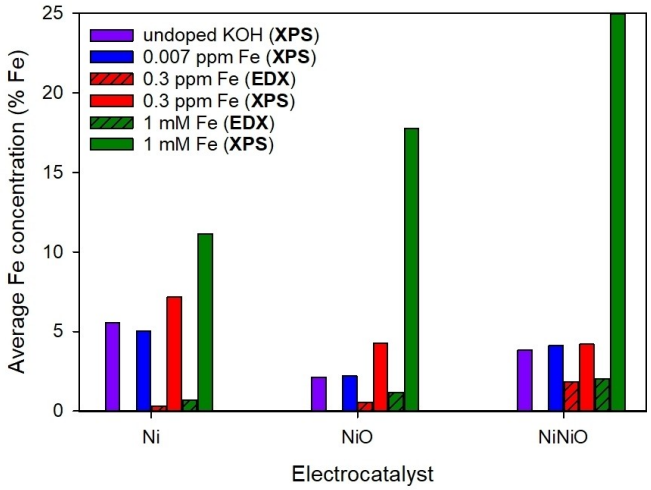

Figure 3. Fe concentrations in the bulk (EDX) and on the surface (XPS) of sputtered Ni electrocatalysts after cycling in KOH containing Fe (EDX results for samples cycled in undoped KOH and 0.007 ppm Fe are excluded because this is below the detection limit of the instrument).

fact that Fe was found to be present as α-FeOOH shows that it is low coordination Fe that is present, and not bulk (high coordination Fe). Therefore, the fact that Fe is found to be present only in the topmost layers of the sputtered thin films is a strong indication that Fe is present only on the surface of the films and not in the bulk.

The concentration of Fe detected by XPS is predominantly one order of magnitude higher than that detected by EDX. The average Fe concentration found within the surfaces of sputtered Ni, NiO and NiNiO, cycled in 0.3 ppm Fe, were 7.15%, 4.27% and 4.19%, respectively. These concentrations were found to be 0.32%, 0.54% and 1.85% by EDX. For Ni, NiO and NiNiO cycled in 1 mM, XPS results showed an average of 11.15%, 17.76% and 26.85% Fe, respectively. The EDX results in turn indicated average values of 0.68%, 1.18% and 2.03%. This clearly shows that the greatest portion of Fe is found within the surface of these samples.

The amounts of Fe observed through XPS are in good agreement with what was previously reported for similar studies. Klaus *et al.* reported that 5% Fe was present in Ni samples after 12 CV cycles in 1 M reagent-grade KOH ($\leq$0.66 ppm Fe). The current study reports similar Fe concentrations for sputtered Ni, NiO and NiNiO cycled in semiconductor-grade KOH as well as 0.3 ppm Fe. Nardi *et al.* reported that between 10 and 15% Fe was present in NiO samples that were cycled in Fe saturated KOH.[9] This is in agreement with sputtered Ni and NiO in this study. Lastly, Burke Stevens *et al.* reported in their work that Ni samples cycled 100 times in 1 mM Fe contained 25% Fe,[5] which is similar to what was found for sputtered NiNiO.

In our work, the amount of Fe within the surface of sputtered NiNiO was found to be the greatest of all sputtered samples. Klaus *et al.* reported that Ni electrocatalysts become saturated with Fe at close to 20% Fe,[4] and it is also reported that co-deposited NiFe electrocatalysts containing 5% and 25% Fe have similar activities.[3] A study on the surface composition of stainless steel also found that the optimum OER activity is found at a composition of around 27% Fe and 73% Ni.[47] Furthermore, He *et al.* found that Fe transitions to a high spin state near the solubility limit of Fe in NiOOH (25%) and that the low spin-state present at lower concentrations of Fe contributes to the excellent OER activity.[48] The results of our study are in accordance with these previously reported findings. For example, NiNiO cycled in 0.3 ppm Fe contains 4.19% Fe and NiNiO cycled in 1 mM contain 26.85% Fe. Even though this is a large difference in Fe content, the overpotentials of these two samples are not drastically different, as evidenced from Figure 6. The same holds true for Ni and NiO. The highest concentration of Fe detected in one of the catalysts studied here is in fact just above the reported solubility limit.

Fe also affects the level of Ni oxidation and the XPS results show that cycling in 1 mM Fe causes the samples to be less oxidised, which could result from the high percentage of Fe present within the surface of these samples.

Electrochemical characterization

The electrochemical behaviour of the 50 nm thick sputtered films of Ni, NiO and NiNiO were investigated in 1 M undoped KOH and six different Fe concentrations, i.e. 0.003 ppm, 0.007 ppm, 0.09 ppm, 0.9 ppm, 0.3 ppm and 1 mM. The 30th cycle for each Ni-type thin film sample within all Fe concentrations are shown in Figure 4. All 30 CV cycles for all samples are shown in Figure S6. The oxidation peak of Ni shifts to more negative potentials as the Fe concentration increases from zero to 0.09 ppm Fe.

Ni cycled in 0.9 ppm Fe and 1 mM Fe have oxidation waves that are shifted to more positive potentials with respect to that of the sample cycled in 0.3 ppm. Some of the samples show the presence of anodic and cathodic peak doublets. Ni samples cycled in 0.3 ppm, 0.9 ppm and 1 mM have cathodic peak shoulders, and anodic peaks that appear to consist of two peaks that are not well split. NiO have shoulders on the anodic and cathodic peaks for samples that have been cycled in KOH containing 0.3 ppm, 0.9 ppm and 1 mM Fe. For both Ni and NiO, the anodic and cathodic peak shoulders seem to be linked to higher Fe content as they are only present from 0.3 ppm Fe and higher. However, NiNiO only have a single oxidation and reduction feature for all of the Fe concentrations.

The most important thing to gather from the oxidation features is that they do not consistently shift positively with increased iron concentration, if the shoulder is not considered. However, when higher concentrations of iron are present, such as 1 mM Fe, an anodic shift is observed. This could indicate that there is Fe inclusion taking place deeper into the bulk of the film. It is reported that when Fe is incorporated into the bulk, the oxidation peak will shift anodically as the Fe concentration increases.[4] Since this does not consistently happen, the redox features might indicate that Fe is not incorporated into the bulk structure for all Fe concentrations and that the changes observed in the CVs are linked to changes on the surface. As we

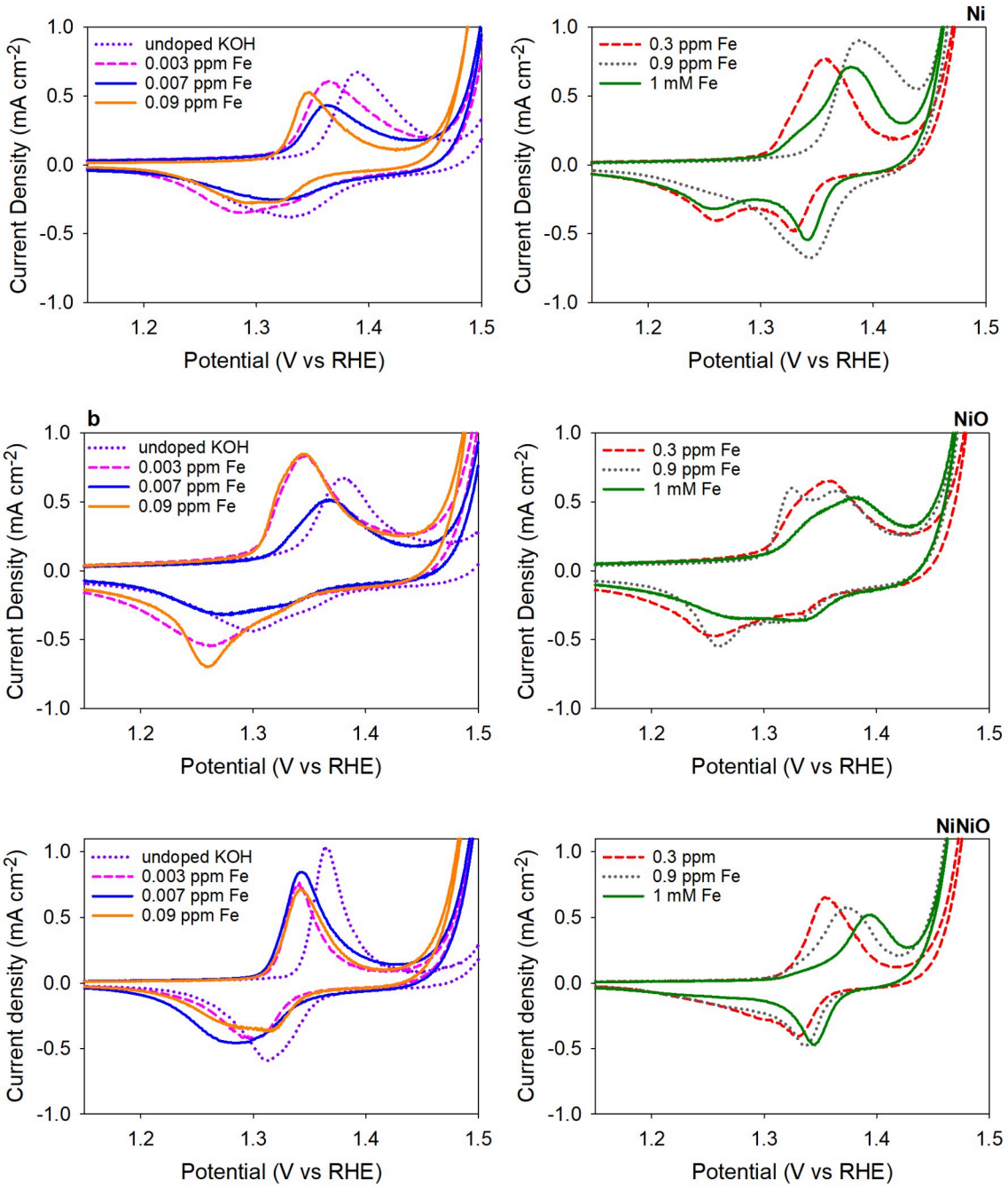

Figure 4. Redox features of the 30th CV cycles at 20 mV s^{-1} of sputtered (a) Ni, (b) NiO and (c) NiNiO in (a) undoped KOH (purple) and KOH containing 0.003 ppm Fe (pink) and 0.007 ppm Fe (blue) and (b) 0.09 ppm Fe (orange) 0.3 ppm Fe (red), 0.9 ppm Fe (grey) and 1 mM Fe (green).

also observed from XPS, not all changes that occur on the surface will result in an increased activity. This also shows that it might be possible that Fe incorporates deeper into the film as the Fe concentration is increased.

LSVs of Ni, NiO, and NiNiO, after 30 CV cycles within each electrolyte composition, can be observed in Figure 5. As the concentration of Fe in the electrolyte increases, so does the OER activity. The overpotential at 10 mA cm^{-2} has been obtained from the LSVs (Figure 5) and these values are summarised in the form of a bar chart in Figure 6. For Ni the overpotentials at 10 mA cm^{-2} are 346 mV, 326 mV, 315 mV, 305 mV, 293 mV, 284 mV and 282 mV in the order of increasing Fe concentration. This clearly shows that the overpotential decreases with increasing Fe concentration. For NiO the overpotentials at 10 mA cm^{-2} are 346 mV, 331 mV, 329 mV, 302 mV, 301 mV, 295 mV and 292 mV, in the order of increasing Fe concentration; with the overpotential also decreasing with increasing Fe concentration, although the overpotential is only slightly higher at greater Fe concentrations. Lastly, for NiNiO the overpotentials at 10 mA cm^{-2} also decrease with increasing

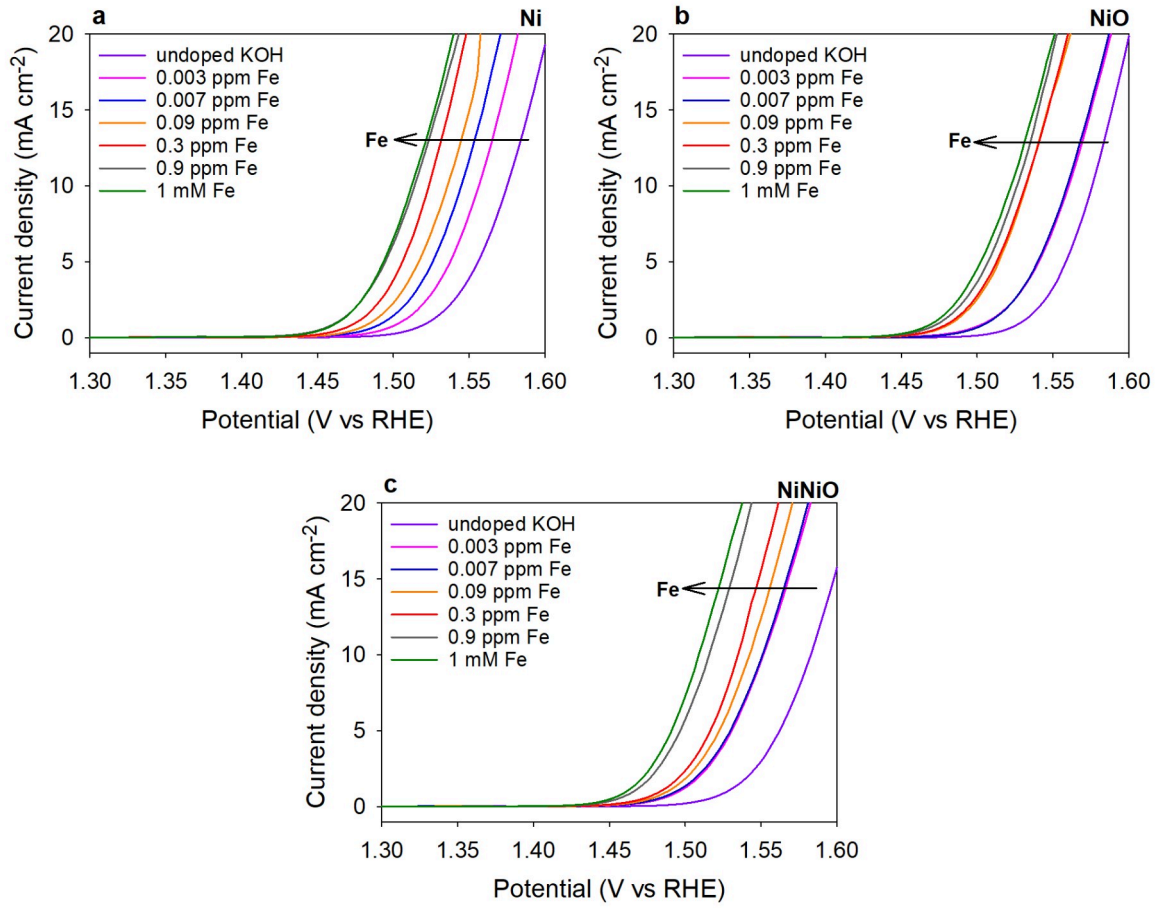

Figure 5. LSVs at 1 mV s^{-1} of sputtered (a) Ni, (b) NiO, and (c) NiNiO, after 30 CVs in undoped KOH (purple), and KOH containing six different concentrations of Fe.

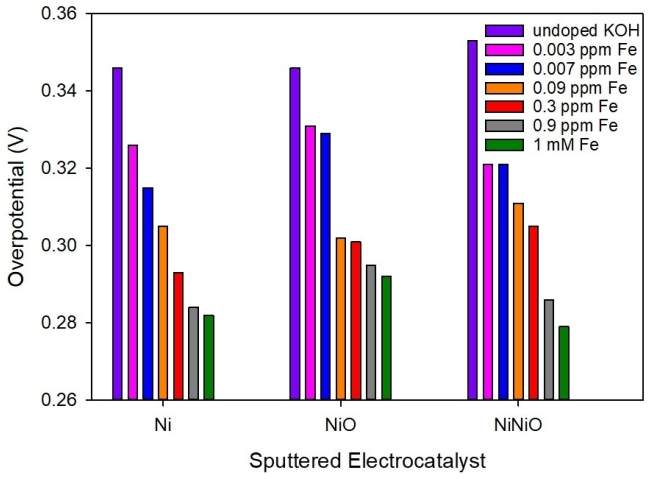

Figure 6. A bar chart summarising the overpotential values of sputtered Ni, NiO, and NiNiO, after 30 CV cycles in KOH containing different concentrations of Fe.

Fe concentration and are 353 mV, 321 mV, 321 mV, 311 mV, 305 mV, 286 mV and 279 mV, starting from undoped KOH and in the order of increasing Fe concentration. The lowest overpotential for each of Ni, NiO, and NiNiO are within 16 mV of one another, which clearly shows that NiNiO, having the lowest overpotential is not vastly superior compared to Ni and NiO.

The Tafel slopes are determined from the slopes of the straight-line plots of the overpotential versus the logarithm of the absolute value of the current density. The RDE was rotated at 1600 rpm for these measurements. The Tafel slopes for the Ni and NiO electrocatalysts are all between 36 mV/dec and 45 mV/dec (Figure 7). These values all correspond with Ni that has been cycled in KOH containing Fe,[49,4] or NiFe electrocatalysts.[14,10,50,51] The Tafel slopes of NiNiO are also comparable with values ranging between 38 mV/dec and 44 mV/dec. This is a narrow range and the values correspond once again with that of previous studies where Ni electrocatalysts are present with Fe.[14,10,50]

To further investigate the electrochemical properties of the different electrocatalysts in electrolytes containing different amounts of Fe, EIS was conducted. The Nyquist plots for the samples are displayed in Figures S7, S8, and S9. A single semicircle is present for each sample at each potential. This means that the entire GC substrate is covered with the sputtered thin film and that we are solely observing the kinetics of the Ni thin film.[52] Furthermore, an equivalent circuit comprised of a solution resistance in series with a parallel combination of a

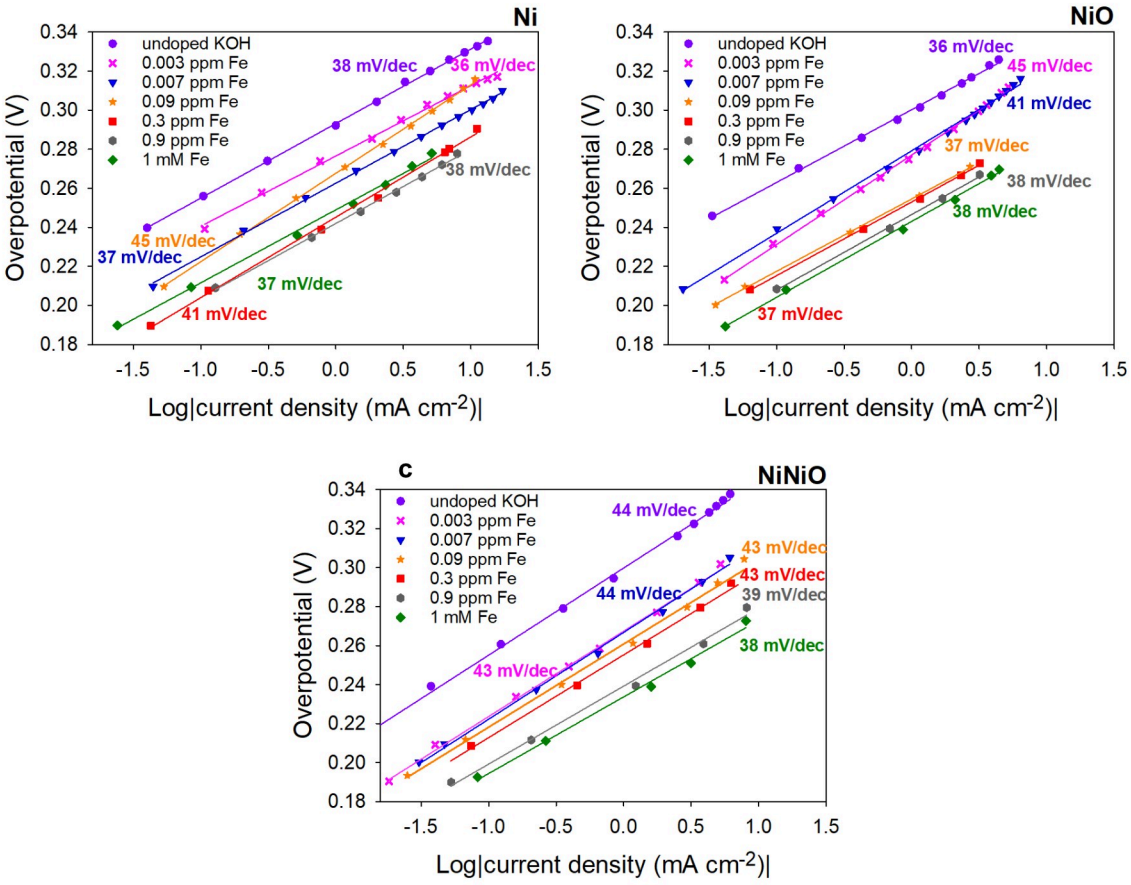

Figure 7. Tafel plots for sputtered (a) Ni, (b) NiO and (c) NiNiO after cycling in undoped KOH and KOH containing six different Fe concentrations.

charge transfer resistance and a double layer capacitance was used to fit the impedance data.

From Figure 8, it is clear that the R_{ct} for each electrocatalyst at each potential value decreases as the Fe concentration increases. The R_{ct}-value at 1.5 V (where the most appreciable OER activity is observed) is 178 Ω after Ni was cycled in undoped KOH. This value decreases all the way to 31 Ω when Ni is cycled in KOH containing 1 mM Fe. It is clear that the addition of Fe to the KOH electrolyte decreases the R_{ct} of Ni electrocatalysts. It is interesting to note that the R_{ct} of NiO samples cycled in 0.003 ppm Fe and 0.007 ppm Fe are similar, while the NiO samples cycled in 0.09 ppm Fe, 0.3 ppm Fe and 0.9 ppm Fe have similar R_{ct}-values. At 1.5 V, the R_{ct} of NiO decreases form 163 Ω for the sample cycled in undoped KOH to 40 Ω for the sample cycled in KOH containing 1 mM Fe. In turn, the R_{ct} at 1.5 V decreases from 105 Ω when NiNiO is cycled in undoped KOH to 26 Ω when NiNiO is cycled in 1 mM Fe. The NiNiO samples cycled in 0.003 ppm Fe and 0.007 ppm Fe have almost the same R_{ct}, similar to that of Ni and NiO.

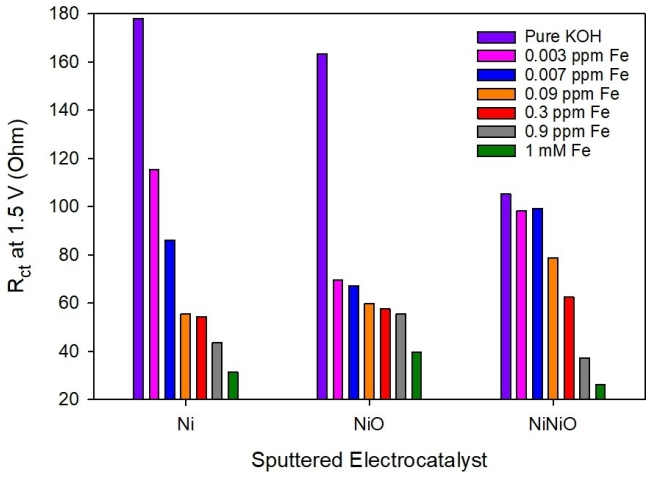

Figure 8. A bar chart of the charge transfer resistance at 1.5 V for sputtered Ni, NiO, and NiNiO in KOH containing different concentrations of Fe.

From Figure 8 it is clear that increased amounts of Fe in the electrolyte decreases the R_{ct} continually up until the point where the electrolyte is saturated with Fe. This emphasizes the strong effect that the amount of Fe in the electrolyte, and subsequently within the top layers of the nickel-based electrocatalysts, has on the kinetics of the OER.

Conclusions

Ni, NiO, and NiNiO, were successfully and reproducibly sputtered on GC substrates allowing for the characterization of

the samples in KOH containing different concentrations of Fe. It was revealed that increasing concentrations of Fe in the alkaline electrolyte increasingly improves the OER activity and decreases the charge transfer resistance of these Ni-based electrocatalysts. Furthermore, XPS and EDX results show that this increase in OER activity, and associated reduction in the charge transfer resistance, is linked to Fe that is present in the top layers of these electrocatalysts that is not found in the deeper layers (beyond the range probed by XPS) of the sample. XPS also indicates that samples cycled in concentrated (1 mM) Fe are less oxidized after cycling and contains significantly more Fe within the surface than samples cycled in lower Fe concentrations. Although these drastic differences are observed for the samples cycled in 0.9 ppm Fe and 1 mM Fe, they exhibit similar OER activities, with the sample cycled in 1 mM Fe having only a slightly lower overpotential. Changes in the redox features are also observed, but they are not necessarily linked to OER activity. This indicates that not all changes/features observed in the electronic structure of electrocatalysts can be linked to OER activity. Some changes occur as an effect of the presence of Fe without having an impact on activity. Lastly, regardless of the starting oxidation state of the Ni-based electrocatalysts (Ni, NiO or NiNiO) they all have similar OER activities. NiNiO seems to incorporate more Fe into its structure than the other two oxidation states (Ni and NiO). The electrocatalytic Fe concentration is the largest contributor to enhanced OER activity and this improvement results from Fe that is present within the top layers of the electrocatalysts after cycling.

Acknowledgements

This work was performed within the SANOCEAN project (South Africa/Norway joint research programme on ocean research including blue economy, climate change, the environment and sustainable energy). The project is financially supported by the National Research Foundation of South Africa (NRF) and the Research Council of Norway (288590). This work is based on the research supported wholly/in part by the National Research Foundation of South Africa (Grant Numbers: 123025, 118753). The Grantholder acknowledges that opinions, findings and conclusions or recommendations expressed in any publication generated by the NRF supported research is that of the author(s) alone, and that the NRF accepts no liability whatsoever in this regard. The SEM and EDX analyses were conducted by Innocent Shuro, materials characterization specialist at the NWU. XPS measurements in this study were performed by Martin F. Sunding at SINTEF materials physics in Oslo.

Conflict of Interests

The authors declare no conflict of interest.

Data Availability Statement

The data that support the findings of this study are available from the corresponding author upon reasonable request.

Keywords: thin film electrocatalysts · magnetron sputtering · oxygen evolution reaction (OER) · hydrogen · iron-containing electrolyte

[1] S. Anantharaj, S. Kundu, S. Noda, *Nano Energy* **2021**, *80*, 105514.
[2] L. Fan, B. Zhang, B. J. J. Timmer, N. V. R. A. Dharanipragada, X. Sheng, C.-W. Tai, F. Zhang, T. Liu, Q. Meng, A. K. Inge, *Nano Energy* **2020**, *72*, 104656.
[3] L. Trotochaud, S. L. Young, J. K. Ranney, S. W. Boettcher, *J. Am. Chem. Soc.* **2014**, *136*, 6744–6753.
[4] S. Klaus, Y. Cai, M. W. Louie, L. Trotochaud, A. T. Bell, *J. Phys. Chem. C* **2015**, *119*, 7243–7254.
[5] M. Burke Stevens, C. D. M. Trang, L. J. Enman, J. Deng, S. W. Boettcher, *J. Am. Chem. Soc.* **2017**, *139*, 11361–11364.
[6] D. A. Corrigan, *J. Electrochem. Soc.* **1987**, *134*, 377.
[7] B. Siang Yeo, A. T. Bell, *J. Phys. Chem. C* **2012**, *116*, 8394–8400.
[8] L.-A. Stern, X. Hu, *Faraday Discuss.* **2015**, *176*, 363–379.
[9] K. L. Nardi, N. Yang, C. F. Dickens, A. L. Strickler, S. F. Bent, *Adv. Energy Mater.* **2015**, *5*, 1500412.
[10] M. W. Louie, A. T. Bell, *J. Am. Chem. Soc.* **2013**, *135*, 12329–12337.
[11] J. Landon, E. Demeter, N. Inoglu, C. Keturakis, I. E. Wachs, R. Vasic, A. I. Frenkel, J. R. Kitchin, *ACS Catal.* **2012**, *2*, 1793–1801.
[12] R. Farhat, J. Dhainy, L. I. Halaoui, *ACS Catal.* **2019**, *10*, 20–35.
[13] D. Y. Chung, P. P. Lopes, P. F. B. D. Martins, H. He, T. Kawaguchi, P. Zapol, H. You, D. Tripkovic, D. Strmcnik, Y. Zhu, *Nat. Energy* **2020**, *5*, 222–230.
[14] R. Wang, C. Wang, S. Yin, Y. Peng, J. Chen, Y. Deng, J. Li, *Catal. Today* **2020**, *364*.
[15] M. E. G. Lyons, M. P. Brandon, *Int. J. Electrochem. Sci.* **2008**, *3*, 1386–1424.
[16] M. F. Kibria, M. S. Mridha, *Int. J. Hydrogen Energy* **1996**, *21*, 179–182.
[17] F. Hahn, B. Beden, M. J. Croissant, C. Lamy, *Electrochim. Acta* **1986**, *31*, 335–342.
[18] K. Juodkazis, J. Juodkazytė, R. Vilkauskaitė, V. Jasulaitienė, *J. Solid State Electrochem.* **2008**, *12*, 1469–1479.
[19] D. A. Wruck, M. A. Dixon, M. Rubin, S. N. Bogy, *J. Vac. Sci. Technol. A: Vacuum, Surfaces, and Films* **1991**, *9*, 2170–2173.
[20] A. Karpinski, A. Ferrec, M. Richard-Plouet, L. Cattin, M. A. Djouadi, L. Brohan, P.-Y. Jouan, *Thin Solid Films* **2012**, *520*, 3609–3613.
[21] D. Friebel, M. W. Louie, M. Bajdich, K. E. Sanwald, Y. Cai, A. M. Wise, M.-J. Cheng, D. Sokaras, T.-C. Weng, R. Alonso-Mori, *J. Am. Chem. Soc.* **2015**, *137*, 1305–1313.
[22] S. Carenco, C. Boissière, L. Nicole, C. Sanchez, P. Le Floch, N. Mézailles, *Chem. Mater.* **2010**, *22*, 1340–1349.
[23] S. Carenco, *Chem. Rec.* **2018**, *18*, 1114–1124.
[24] M. K. Bates, Q. Jia, N. Ramaswamy, R. J. Allen, S. Mukerjee, *J. Phys. Chem. C* **2015**, *119*, 5467–5477.
[25] A. Y. Faid, A. O. Barnett, F. Seland, S. Sunde, *Electrochim. Acta* **2020**, *361*, 137040.
[26] I. M. Sadiek, A. M. Mohammad, M. E. El-Shakre, M. S. El-Deab, *Int. J. Hydrogen Energy* **2012**, *37*, 68–77.
[27] F. Chekin, H. Tahermansouri, M. R. Besharat, *J. Solid State Electrochem.* **2014**, *18*, 747–753.
[28] S. Anantharaj, P. E. Karthik, S. Kundu, *Catal. Sci. Technol.* **2017**, *7*, 882–893.
[29] K. Karthick, S. Subhashini, R. Kumar, S. Sethuram Markandaraj, M. M. Teepikha, S. Kundu, *Inorg. Chem.* **2020**, *59*, 16690–16702.
[30] M. Tahir, L. Pan, F. Idrees, X. Zhang, L. Wang, J.-J. Zou, Z. L. Wang, *Nano Energy* **2017**, *37*, 136–157.
[31] A. G. Oshchepkov, A. Bonnefont, E. R. Savinova, *Electrocatalysis* **2020**, *11*, 133–142.

[32] Y. Dong, J. Dang, W. Wang, S. Yin, Y. Wang, *ACS Appl. Mater. Interfaces* **2018**, *10*, 39624–39630.
[33] F. Song, L. Bai, A. Moysiadou, S. Lee, C. Hu, L. Liardet, X. Hu, *J. Am. Chem. Soc.* **2018**, *140*, 7748–7759.
[34] K. Fominykh, J. M. Feckl, J. Sicklinger, M. Döblinger, S. Böcklein, J. Ziegler, L. Peter, J. Rathousky, E. Scheidt, T. Bein, *Adv. Funct. Mater.* **2014**, *24*, 3123–3129.
[35] F. Portemer, A. Delahaye-Vidal, M. Figlarz, *J. Electrochem. Soc.* **1992**, *139*, 671.
[36] E. L. Miller, R. E. Rocheleau, *J. Electrochem. Soc.* **1997**, *144*, 3072–3077.
[37] R. J. Kriek, L. A. van Heerden, A. Falch, M. I. Gillespie, A. Y. Faid, F. Seland, *J. Power Sources* **2021**, *494*, 229344.
[38] C. Kjartansdóttir, M. Caspersen, S. Egelund, P. Møller, *Electrochim. Acta* **2014**, *142*, 324–335.
[39] P. Chen, L.-K. Wang, G. Wang, M.-R. Gao, J. Ge, W.-J. Yuan, Y.-H. Shen, A.-J. Xie, S.-H. Yu, *Energy Environ. Sci.* **2014**, *7*, 4095–4103.
[40] K. Oldham, J. Myland, A. Bond, *Electrochemical Science and Technology: Fundamentals and Applications*, John Wiley & Sons **2011**.
[41] C. Roy, B. Sebok, S. B. Scott, E. M. Fiordaliso, J. E. Sørensen, A. Bodin, D. B. Trimarco, C. D. Damsgaard, P. C. K. Vesborg, O. Hansen, I. E. L. Stephens, J. Kibsgaard, I. Chorkendorff, *Nat. Catal.* **2018**, *1*, 820–829.
[42] M. Steimecke, G. Seiffarth, C. Schneemann, F. Oehler, S. Förster, M. Bron, *ACS Catal.* **2020**, *10*, 3595–3603.
[43] S. Fu, J. Song, C. Zhu, G.-L. Xu, K. Amine, C. Sun, X. Li, M. H. Engelhard, D. Du, Y. Lin, *Nano Energy* **2018**, *44*, 319–326.
[44] S. Dutta, A. Indra, Y. Feng, T. Song, U. Paik, *ACS Appl. Mater. Interfaces* **2017**, *9*, 33766–33774.
[45] A. Liu, G. Liu, H. Zhu, B. Shin, E. Fortunato, R. Martins, F. Shan, *Appl. Phys. Lett.* **2016**, *108*, 233506.
[46] M. M. Heath, F. Poureshghi, F. Seland, S. Sunde, R. J. Kriek, *Energy Technol.* **2023**, *11*, 2300313.
[47] H. R. Zamanizadeh, S. Sunde, B. G. Pollet, F. Seland, *Electrochim. Acta* **2022**, *424*, 140561.
[48] Z.-D. He, R. Tesch, M. J. Eslamibidgoli, M. H. Eikerling, P. M. Kowalski, *Nat. Commun.* **2023**, *14*, 3498.
[49] K. Wan, J. Luo, X. Zhang, P. Subramanian, J. Fransaer, *Int. J. Hydrogen Energy* **2020**, *45*, 8490–8496.
[50] L. Bai, S. Lee, X. Hu, *Angew. Chem.* **2020**, *133*, 3132–3140.
[51] H.-S. Hu, S. Si, R.-J. Liu, C.-B. Wang, Y.-Y. Feng, *Int. J. Energy Res.* **2020**, *44*, 9222–9232.
[52] S. Anantharaj, S. Noda, *ChemElectroChem* **2020**, *7*, 2297–2308.

Manuscript received: September 21, 2023
Revised manuscript received: December 7, 2023
Version of record online: January 22, 2024